AD-A074 949 PROTOTYPE DEVELOPMENT ASSOCIATES INC SANTA ANA CA F/G 16/4
PRELIMINARY ASSESSMENT OF VULNERABILITY OF TACTICAL MISSILE MAT--ETC(U)
OCT 78 E C ALEXANDER DNA001-78-C-0248
UNCLASSIFIED PDA-TR-1418-00-02 DNA-4765F NL

| OF |
AD A074949

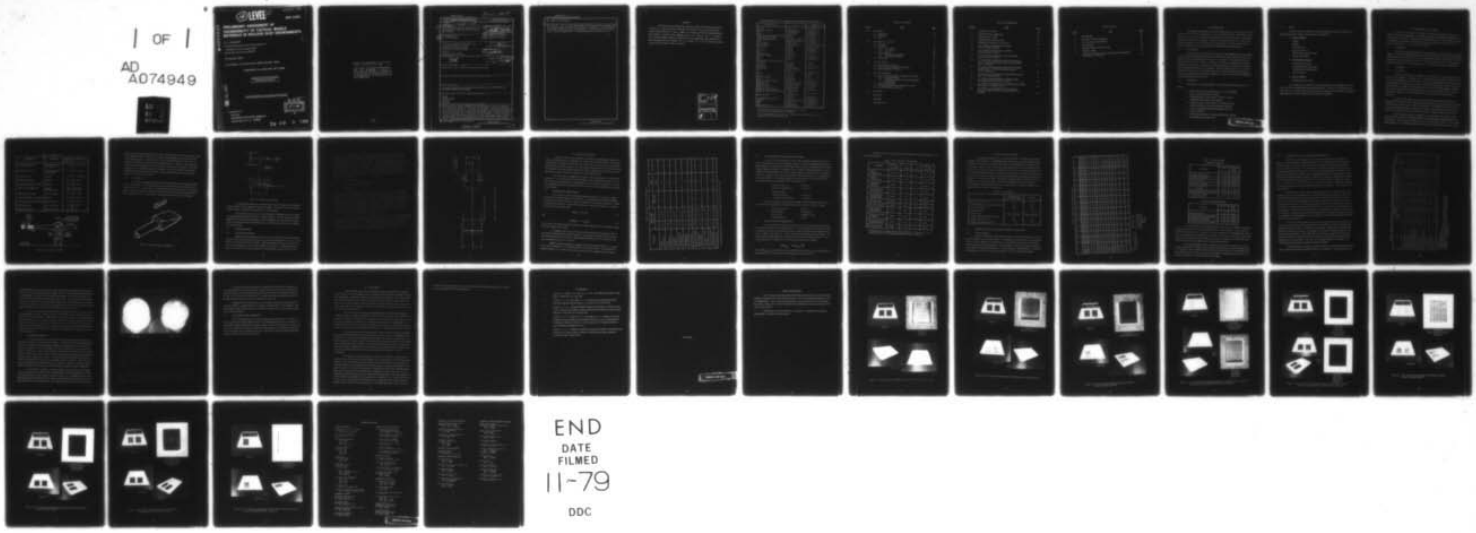

END
DATE FILMED
11-79
DDC

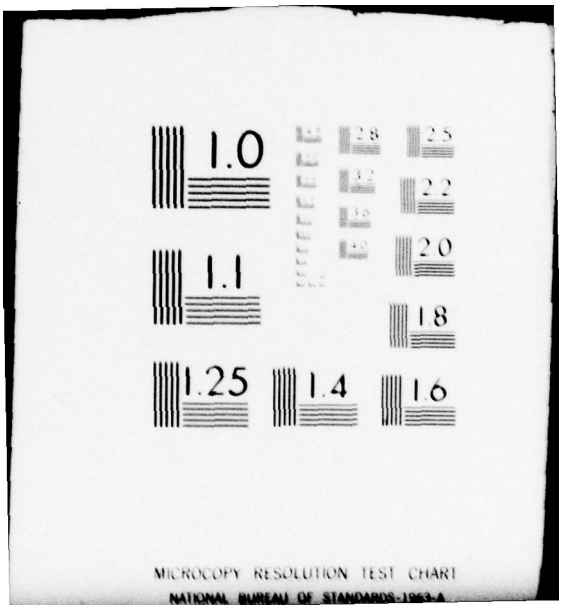
1.0
1.1
1.25
1.4
1.6
2.2
2.0
1.8
MICROCOPY RESOLUTION TEST CHART
NATIONAL BUREAU OF STANDARDS-1963-A

(12) LEVEL III

DNA 4765F

PRELIMINARY ASSESSMENT OF VULNERABILITY OF TACTICAL MISSILE MATERIALS IN NUCLEAR DUST ENVIRONMENTS

E. C. Alexander

Prototype Development Associates, Inc.

1740 Garry Avenue, Suite 201

Santa Ana, California 92705

31 October 1978

Final Report for Period April 1978—October 1978

CONTRACT No. DNA 001-78-C-0248

APPROVED FOR PUBLIC RELEASE;
DISTRIBUTION UNLIMITED.

THIS WORK SPONSORED BY THE DEFENSE NUCLEAR AGENCY
UNDER RDT&E RMSS CODE B342078464 N99QAXAI12906 H2590D.

Prepared for

Director

DEFENSE NUCLEAR AGENCY

Washington, D. C. 20305

Destroy this report when it is no longer needed. Do not return to sender.

PLEASE NOTIFY THE DEFENSE NUCLEAR AGENCY, ATTN: STTI, WASHINGTON, D.C. 20305, IF YOUR ADDRESS IS INCORRECT, IF YOU WISH TO BE DELETED FROM THE DISTRIBUTION LIST, OR IF THE ADDRESSEE IS NO LONGER EMPLOYED BY YOUR ORGANIZATION.

UNCLASSIFIED

SECURITY CLASSIFICATION OF THIS PAGE (When Data Entered)

(18) DNA, SBIE

(19) **REPORT DOCUMENTATION PAGE**

READ INSTRUCTIONS BEFORE COMPLETING FORM

1. REPORT NUMBER: DNA 4765F — 2. GOVT ACCESSION NO.: AD-E300 592 — 3. RECIPIENT'S CATALOG NUMBER:

(6) 4. TITLE (and Subtitle): PRELIMINARY ASSESSMENT OF VULNERABILITY OF TACTICAL MISSILE MATERIALS IN NUCLEAR DUST ENVIRONMENTS.

(9) 5. TYPE OF REPORT & PERIOD COVERED: Final Report for Period Apr 78 – October 1978

(14) 6. PERFORMING ORG. REPORT NUMBER: PDA-TR-1418-00-02

(10) 7. AUTHOR(s): E. C. Alexander

(15) 8. CONTRACT OR GRANT NUMBER(s): DNA 001-78-C-0248

9. PERFORMING ORGANIZATION NAME AND ADDRESS:
Prototype Development Associates, Inc.
1740 Garry Avenue, Suite 201
Santa Ana, California 92705

(16) 10. PROGRAM ELEMENT, PROJECT, TASK AREA & WORK UNIT NUMBERS: NWED Subtask N99QAXAI129-06

(11) 11. CONTROLLING OFFICE NAME AND ADDRESS:
Director
Defense Nuclear Agency
Washington, D. C. 20305

12. REPORT DATE: 31 October 1978

13. NUMBER OF PAGES: 46

14. MONITORING AGENCY NAME & ADDRESS (if different from Controlling Office): (12) 45

15. SECURITY CLASS (of this report): UNCLASSIFIED (17) I 129

15a. DECLASSIFICATION DOWNGRADING SCHEDULE

16. DISTRIBUTION STATEMENT (of this Report)

Approved for public release; distribution unlimited.

17. DISTRIBUTION STATEMENT (of the abstract entered in Block 20, if different from Report)

18. SUPPLEMENTARY NOTES

This work sponsored by the Defense Nuclear Agency under RDT&E RMSS Code B342078464 N99QAXAI12906 H2590D.

19. KEY WORDS (Continue on reverse side if necessary and identify by block number)

Radome
Antenna Window
Erosion
Materials

20. ABSTRACT (Continue on reverse side if necessary and identify by block number)

Erosion tests of several candidate electromagnetic and optical window materials were performed at the AEDC Dust Erosion Tunnel. The test conditions were selected to simulate: 1) operational conditions that may be experienced by tactical missiles in a nuclear dust environment, and 2) conditions used in tests of these materials in simulated rain environments. Alumina and beryllia were found to be the most erosion-resistant radome materials in the conditions tested, while 1D Celcon/quartz was the best antenna window material. It also was found that the measured dust erosion rates were significantly

over

DD FORM 1 JAN 73 1473 EDITION OF 1 NOV 65 IS OBSOLETE

UNCLASSIFIED

SECURITY CLASSIFICATION OF THIS PAGE (When Data Entered)

390 714

1/3

20. Abstract (Continued)

different than the rates that would be predicted on the basis of rain erosion test results. Tests also were performed on two magnesium fluoride domes used in conjunction with infrared sensor systems. Exposure to a relatively mild erosive environment was found to compromise the survivability of this material, as well as degrading its infrared transmission characteristics.

PREFACE

The test program described in this report was conducted by Prototype Development Associates, Inc. (PDA), Santa Ana, California, for the Defense Nuclear Agency (DNA) under Contract Number DNA001-78-C-0248. Captain A. T. Hopkins was the DNA Contracting Officer's Representative. The PDA Program Manager was Mr. M. M. Sherman. Mr. E. C. Alexander was the Principal Engineer and was responsible for the test engineering, data reduction, and data evaluation phases of the program. Mr. G. F. Schmitt, Jr., Air Force Materials Laboratory, provided material samples for the experiments.

Conversion factors for U. S. customary to metric (SI) units of measurement.

To Convert From	To	Multiply By
angstrom	meters (m)	1.000 000 X E -10
atmosphere (normal)	kilo pascal (kPa)	1.013 25 X E +2
bar	kilo pascal (kPa)	1.000 000 X E +2
barn	meter^2 (m^2)	1.000 000 X E -28
British thermal unit (thermochemical)	joule (J)	1.054 350 X E +3
calorie (thermochemical)	joule (J)	4.184 000
cal (thermochemical)/cm^2	mega joule/m^2 (MJ/m^2)	4.184 000 X E -2
curie	giga becquerel (GBq)*	3.700 000 X E +1
degree (angle)	radian (rad)	1.745 329 X E -2
degree Fahrenheit	degree kelvin (K)	$T_K = (t^o f + 459.67)/1.8$
electron volt	joule (J)	1.602 19 X E -19
erg	joule (J)	1.000 000 X E -7
erg/second	watt (W)	1.000 000 X E -7
foot	meter (m)	3.048 000 X E -1
foot-pound-force	joule (J)	1.355 818
gallon (U. S. liquid)	meter^3 (m^3)	3.785 412 X E -3
inch	meter (m)	2.540 000 X E -2
jerk	joule (J)	1.000 000 X E +9
joule/kilogram (J/kg) (radiation dose absorbed)	Gray (Gy)**	1.000 000
kilotons	terajoules	4.183
kip (1000 lbf)	newton (N)	4.448 222 X E +3
kip/inch^2 (ksi)	kilo pascal (kPa)	6.894 757 X E +3
ktap	newton-second/m^2 ($N-s/m^2$)	1.000 000 X E +2
micron	meter (m)	1.000 000 X E -6
mil	meter (m)	2.540 000 X E -5
mile (international)	meter (m)	1.609 344 X E +3
ounce	kilogram (kg)	2.834 952 X E -2
pound-force (lbf avoirdupois)	newton (N)	4.448 222
pound-force inch	newton-meter (N·m)	1.129 848 X E -1
pound-force/inch	newton/meter (N/m)	1.751 268 X E +2
pound-force/foot^2	kilo pascal (kPa)	4.788 026 X E -2
pound-force/inch^2 (psi)	kilo pascal (kPa)	6.894 757
pound-mass (lbm avoirdupois)	kilogram (kg)	4.535 924 X E -1
pound-mass-foot^2 (moment of inertia)	kilogram-meter^2 ($kg·m^2$)	4.214 011 X E -2
pound-mass/foot^3	kilogram/meter^3 (kg/m^3)	1.601 846 X E +1
rad (radiation dose absorbed)	Gray (Gy)**	1.000 000 X E -2
roentgen	coulomb/kilogram (C/kg)	2.579 760 X E -4
shake	second (s)	1.000 000 X E -8
slug	kilogram (kg)	1.459 390 X E +1
torr (mm Hg, 0^o C)	kilo pascal (kPa)	1.333 22 X E -1

*The becquerel (Bq) is the SI unit of radioactivity; 1 Bq = 1 event/s.

**The Gray (Gy) is the SI unit of absorbed radiation.

A more complete listing of conversions may be found in "Metric Practice Guide E 380-74," American Society for Testing and Materials.

TABLE OF CONTENTS

LIST OF ILLUSTRATIONS

LIST OF TABLES

1.0 INTRODUCTION

The potential vulnerability of aircraft and tactical missiles to rain and dust effects may become more severe as the velocity of these systems continues to increase. Of particular importance is the erosion mass loss experienced by tactical missile radomes, IR domes, and antenna windows in a nuclear dust environment. Prototype Development Associates, Inc. (PDA) has performed a preliminary assessment of the dust erosion behavior of selected electromagnetic and optical window materials in the Vulnerability of Tactical Missile Materials Program.

1.1 BACKGROUND

Prior to the tests performed in this program, an understanding of the erosion behavior of most radome and antenna window materials was limited to erosion in rain environments at the High Speed Test Track at Holloman Air Force Base, New Mexico. While the dust erosion and rain erosion rates of these ceramics were believed to be similar in comparable environments, the hypothesis was untested. Furthermore, erosion data in environments which were representative of a nuclear dust cloud were not available. Thus, the characterization of the dust erosion behavior of the ceramics in representative nuclear dust environments and the relationships between dust erosion and rain erosion were identified as key data requirements for operational and developmental tactical missile systems.

1.2 OBJECTIVES

The objectives of the Vulnerability of Tactical Missile Materials Program were as follows:

1. Obtain relative erosion rate data for each of several candidate radome and antenna window materials.
2. Obtain quantitative erosion behavior data for the ceramic materials in general and for each material.
3. Compare the dust erosion responses of the materials with predicted responses based on existing rain erosion data.
4. Assess the analytical methods for predicting erosion of ceramic materials.
5. Evaluate the performance of one infrared (IR) dome material in a simulated nuclear dust cloud.

1.3 SCOPE

The dust erosion tests included the following candidate materials for potential use as tactical missile system radomes, antenna windows, and IR domes:

- Radome Materials

  Alumina
  Beryllia
  Pyroceram 9606
  Rayceram Cordierite
  Reaction Sintered Silicon Nitride
  Slip Cast Fused Silica

- Antenna Window Materials

  Ethyl Silicate/3D Quartz
  Isotropic Pyrolytic Boron Nitride
  Jelly Roll Quartz/Colloidal Silica
  1D Celcon/Quartz

- IR Dome Material

  Magnesium Fluoride (MgF_2)

The selection of these materials was limited primarily by the availability of test samples from a list of operational and developmental materials. The erosion test environment was defined by a set of conditions which best represented the Holloman rain environments, operational flight conditions, and were within the dust erosion tunnel capabilities.

2.0 DESCRIPTION OF TEST SERIES

The dust erosion tests were conducted at the Arnold Engineering Development Center (AEDC), Dust Erosion Tunnel (DET). This facility was designed specifically as a particle drag accelerator to test the effects of high velocity solid particle impacts on a wide variety of materials. The materials, test apparatus (test facility and model), instrumentation, and test method are discussed in Sections 2.1, 2.2, 2.3 and 2.4, respectively.

2.1 MATERIALS

A list of the candidate materials is presented in Table 1. The list includes the material supplier, density, and an identification code provided with each specimen. All radome and antenna window specimens were provided by the Air Force Materials Laboratory (AFML), and the specimen identifications are those assigned by AFML. Two IR dome samples were tested. One sample was obtained from Hill Air Force Base and the other was purchased directly from the manufacturer.

2.2 APPARATUS

2.2.1 Test Facility

The dust erosion tunnel was designed to accelerate particles to velocities greater than 5000 ft/sec on a continuous (>5 minutes) basis. A schematic plan of the tunnel is shown in Figure 1. Air is heated to high temperatures by an electric arc heater, ducted through a dust injection system, and then expanded in a long nozzle. The air flow exits from the expansion nozzle into a closed test cabin which houses a rotatory model injection system. Nine model mounting stings are available which can be programmed to rotate models into the jet for varied durations. The flow exits the cabin through a diffuser, is ducted into exhaust compressors, and then discharged into the atmosphere.

Pressurized dust hoppers are used to inject particulate matter into the heated air. Materials which have been used to simulate dust are magnesium oxide (50, 100, and 650μm), silicon carbide (100μm), and glass spheres (100, 200, and 650μm). The particle flow rate is determined by the pressure in the dust hopper. This pressure cannot be varied during a run. However, the particle flow duration can be varied from model to model by turning the particle flow on and off.

A laser holographic system is available for characterizing the dust cloud. A single exposed hologram can be used to obtain the particle size distribution and spatial coordinates of the dust particles. A double exposed hologram can be used to obtain particle velocities. Laser shadowgraph equipment also is available but cannot be used concurrently with the laser hologram, since

Table 1. Materials list.

MATERIAL ID	SUPPLIER	DENSITY (gm/cc)	SPECIMEN ID
Alumina (Alsimag 753)	American Lava Div.; 3M Company	3.850	A3-5.0-1,2,3,4
Beryllia (Alsimag 754)	American Lava Div.; 3M Company	2.880	A6-5.0-1,2,3
Pyroceram 9606	Corning	2.599	A1-5.0R-1,2,3,4
Rayceram Cordierite	Raytheon	2.510	A17-5.0-10
Reaction Sintered Silicon Nitride	Raytheon	2.550	A42-5.0R-4
Slip Cast Fused Silica 7941	Corning Martin Marietta	1.950 1.918	A36-5.0R-1 A73-4.0R-4
Ethyl Silicate/3D Quartz	Avco Corporation	1.748	A4-5.0R-7,8
Isotropic Pyrolytic Boron Nitride	Raytheon	1.320	A6-4.0R-6,7
Jelly Roll Quartz/Colloidal Silica	Martin Marietta	1.650	A41-5.0R-2,3
1D Celcon/Quartz	Avco Corporation	1.803	A5-4.0R-8
Magnesium Fluoride	Bausch and Lomb	3.180	SD-3,8

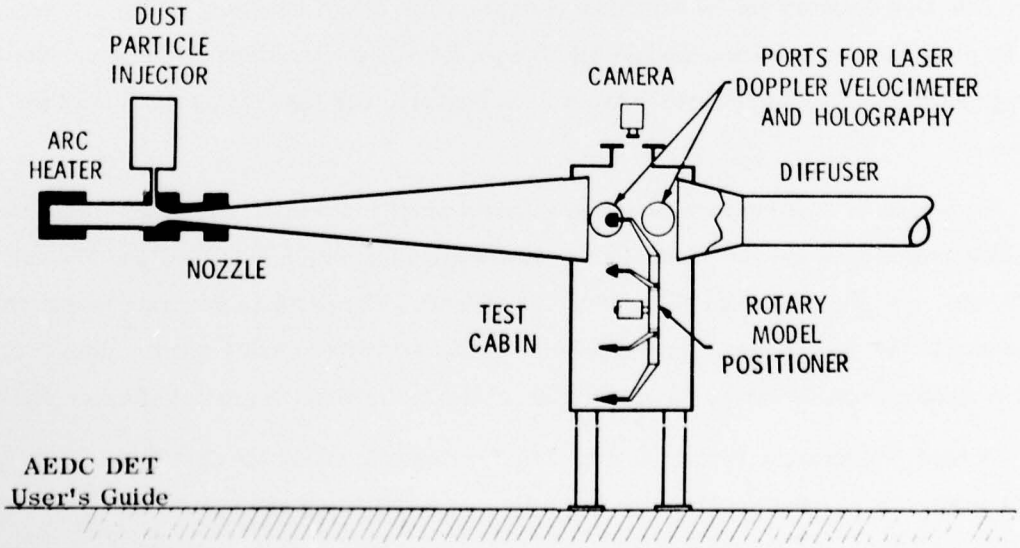

Figure 1. Schematic view of DET.

both use the same optical window in the test cabin. Particle velocities also can be measured using a laser doppler velocimeter (LDV). These particle characterization systems are discussed in more detail in Reference 1. While the laser systems yield good information, state-of-the-art methods for reducing the data are time-consuming and expensive. Therefore, a particle impact bar and high-speed photography are often used to determine the cloud concentration. This information then can be compared to particle mass balance, arc heater performance, and existing calibration data to characterize the dust cloud. None of these particle flow characterization methods were used in the present tests.

2.2.2 Test Model

The radome and antenna window test model configuration was a two-dimensional (2D) wedge, shown in Figure 2. The leading edge is water cooled, while the piece which holds the test specimen is uncooled. A wedge surface assembly is mounted on the 2D wedge to form an erosion surface. The wedge surface assembly, shown in Figure 3, includes two test specimens which are fixed mechanically between a silica phenolic retainer plate and an epoxy glass backing plate.

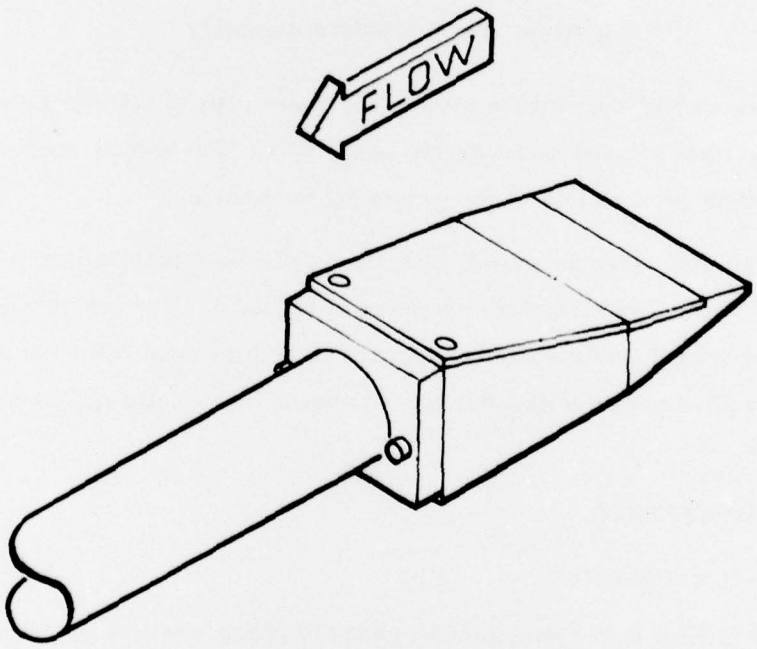

Figure 2. Typical wedge test configuration.

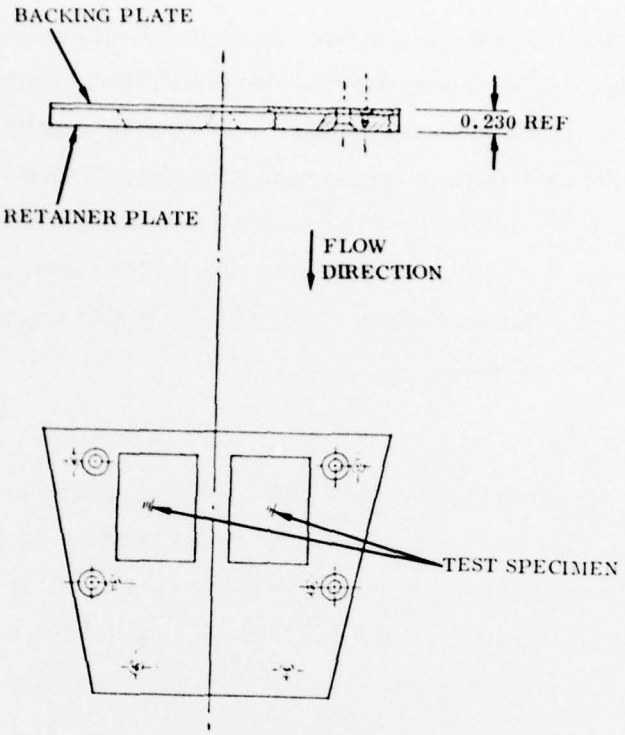

Figure 3. Wedge surface assembly.

Two different 2D wedges were used in the tests. One of the wedges was asymmetric with the single test surface aligned 13.5 degrees to the flow. The second wedge was a 9-degree symmetric wedge. Both sides of this wedge were used for testing.

The two IR dome models were hemisphere-cylinder configurations with the cylinder axis aligned parallel to the flow direction, as shown in Figure 4. The two samples represented slightly different operational configurations, with the main difference reflected in the material thickness: Specimen SD-3 had an initial thickness of 0.109 inch, while Specimen SD-8 initially was 0.160-inch thick.

2.3 INSTRUMENTATION

2.3.1 External Instrumentation

Standard facility instrumentation was used to record the test parameters required to calculate the arc heater performance (arc voltage, current, cooling water flow, ΔT, etc.). These data were recorded on strip chart recorders. Optical thermogage pyrometers were focused on the test specimen midpoint to sense surface brightness temperatures. Voltage output from the pyrometers and other time-dependent parameters (model injection, particle flow, etc.) were

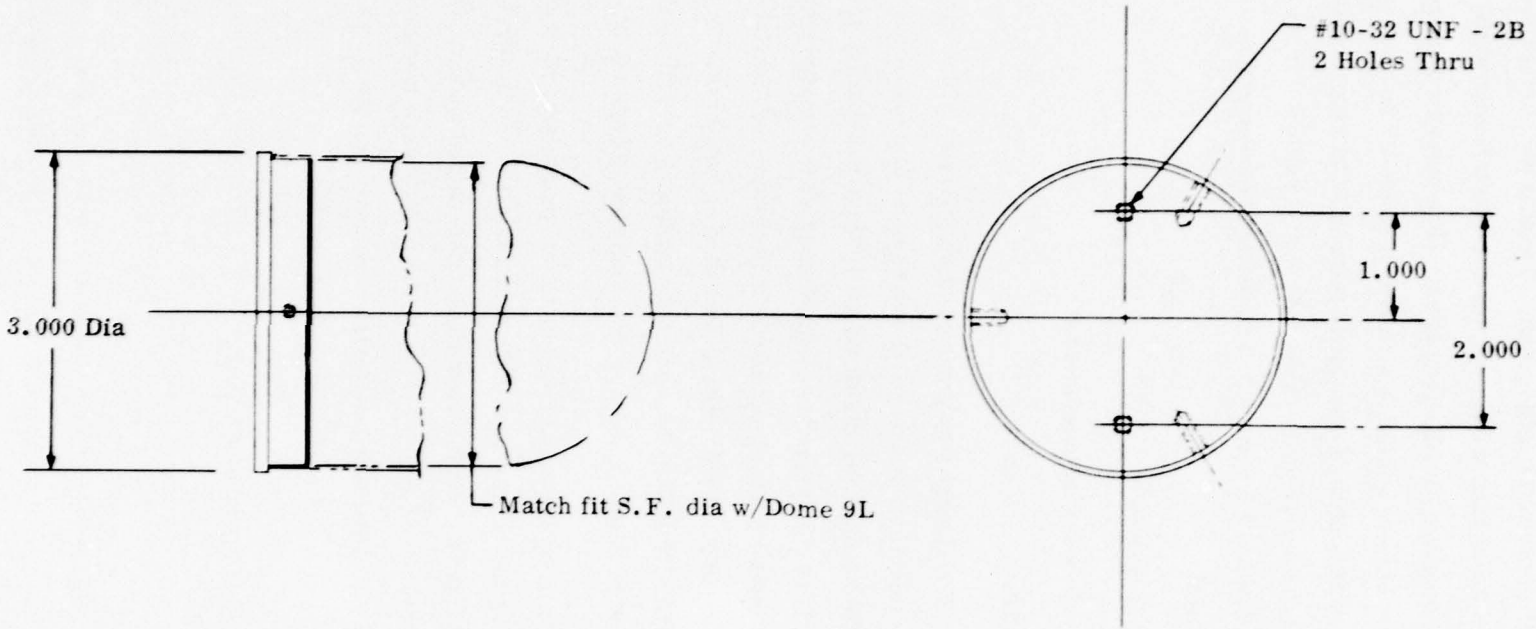

Figure 4. Typical IR dome model assembly.

3.0 PRE-TEST ANALYSES

A literature survey of erosion data for the radome and antenna window materials was made to provide data for pre-test predictions of erosion rates in the DET facility. Because all existing data were obtained from Holloman rain erosion tests, it was necessary to use rain data to estimate the dust erosion response. The dust erosion test parameters were selected to approximate conditions used in the Holloman sled tests in order to minimize the differences between the expected dust erosion results and predictions based on the rain test data.

The rain erosion correlations and the range of rain test parameters are summarized in Section 3.1. The selected dust erosion test parameters are summarized in Section 3.2. Predicted dust erosion rates using the selected parameters are summarized in Section 3.3. No data were available for the IR dome material; therefore, pre-test recession predictions were not made for these models.

3.1 RAIN EROSION CORRELATIONS

An erosion rate-velocity-impingement angle approach has been used by the AFML to correlate rain erosion data (References 2 through 5). A mean depth of penetration rate (MDPR) has been defined in which erosion is assumed to be uniform across the entire sample area. MDPR is calculated from weight loss, density, known surface area, and time of exposure. Two expressions have been used to fit the data:

$$\text{MDPR} = KV^{\alpha}\sin^{2}\theta \tag{1}$$

and

$$\text{MDPR}\sin\theta = K(V\sin\theta)^{\alpha} \tag{2}$$

where K and α are empirical material constants, V is impact velocity, and θ is the particle impingement angle relative to the surface.

A substantial number of tests have been run at the Holloman track facility for each of the radome and antenna window materials of interest. In general, most of the data reviewed were in the velocity range 4000 to 6500 ft/sec, with impingement angles from 13.5 to 60 degrees, and rain concentrations from 2.8 to 7.8 gm/m^3.

MDPR correlation constants are summarized for each material in Table 2. The approximate rain concentrations, ω, for which the data were correlated are listed. The appropriate correlation equation (1 or 2) and the reference from which the data were obtained also are presented.

Table 2. Summary of rain correlation data.

MATERIAL	CORRELATION CONSTANTS		CORRELATION* EQUATION	RAIN CONCENTRATION ω (GM/M^3)	REFERENCE
	α	K			
Alumina (Alsimag 753)	9.496	5.41×10^{-35}	2	2.8	2
Beryllia (Alsimag 754)	4.272	2.81×10^{-17}	2	2.8	2
Ethyl Silicate/ 3D Quartz	3.652	2.21×10^{-13}	1	6.5	3
Isotropic Pyrolytic Boron Nitride	4.643	6.05×10^{-17}	1	7.8	4
Jelly Roll Quartz/ Colloidal Silica	8.429	1.12×10^{-31}	1	6.5	3
Pyroceram 9606	5.595	2.10×10^{-20}	2	3.0	5
Rayceram Cordierite	8.306	1.69×10^{-29}	2	2.8	2
Reaction Sintered Silicon Nitride	3.110	1.92×10^{-12}	2	3.0	3
Slip Cast Fused Silica (Corning)	5.741	9.77×10^{-22}	1	6.5	3
Slip Cast Fused Silica (Martin Marietta)	3.070	6.66×10^{-12}	2	3.0	5
1D Celcon/Quartz	6.539	1.08×10^{-24}	1	6.5	3

*Correlation equation numbers correspond to equation numbers in text of this report.

3.2 DUST EROSION TEST PARAMETERS SELECTION

The dust erosion test parameters for the radome and antenna window materials were selected primarily from the range of available rain data, as well as from anticipated operational flight conditions. Operational and developmental designs of radomes and antenna windows include stagnation impingement angles for uncapped radomes, shallower impingement angles for radomes equipped with metal stagnation caps, and very shallow angles for antenna windows. The tactical missiles are designed to fly at supersonic velocities which can exceed Mach 5. Considering these operational conditions, the following nominal dust erosion parameters were selected from the range of Holloman rain test parameters discussed in Section 3.1:

Particle Velocity, V_p	4300 ft/sec
Particle Concentration, ω_p	3.32 gm/m^3
Impingement Angle	
Radome Materials	13.5 degrees
Antenna Window Materials	9.0 degrees

The flow stagnation pressure and total enthalpy, and the particle type and size then were selected from available DET calibration data to achieve the desired particle velocity.

Chamber Pressure, P_o	1000 psi
Total Enthalpy, h_o	1800 Btu/lbm
Particle Type	Magnesium Oxide
Particle Diameter	200μm

3.3 DUST EROSION RATE PREDICTIONS

Pre-test predictions of the dust erosion rates for the test materials were made using the selected test parameters presented in Section 3.2. These predictions assumed that the MDPR correlations derived for these materials from tests in rain environments could be applied to dust erosion. Another assumption used was that erosion rate varied linearly with concentration. This was reported by Schmitt in Reference 5 for the rain test regime at the Holloman track. A dust erosion rate then was computed in terms of the rain erosion rate by the equation

$$MDPR_{dust} = MDPR_{rain} \times \frac{\omega_p}{\omega},$$

where $MDPR_{rain}$ was determined from the correlation data in Table 2, ω_p is the selected dust concentration (3.32 g/m^3), and ω is the rain concentration reported in Table 2.

Predicted pre-test erosion rates and the test parameters used in the predictions are summarized in Table 3.

Table 3. Pre-test erosion rate predictions.

MATERIAL	$MDPR_{rain}$* (IN/SEC)	ω_p (GM/M^3)	ω (GM/M^3)	$MDPR_{dust}$ (IN/SEC)
Alumina (Alsimag 753)	2.91×10^{-6}	3.32	2.8	3.45×10^{-6}
Beryllia (Alsimag 754)	3.15×10^{-4}	3.32	2.8	3.74×10^{-4}
Ethyl Silicate/ 3D Quartz	0.0400	3.32	6.5	0.0204
Isotropic Pyrolytic Boron Nitride	0.0430	3.32	7.8	0.0183
Jelly Roll Quartz/ Colloidal Silica	0.0046	3.32	6.5	0.0023
Pyroceram 9606	0.0022	3.32	3.0	0.0024
Rayceran Cordierite	0.0002	3.32	2.8	0.0002
Reaction Sintered Silicon Nitride	0.0071	3.32	3.0	0.0079
Slip Cast Fused Silica (Corning)	0.0152	3.32	6.5	0.0191
Slip Cast Fused Silica (Martin Marietta)	0.0185	3.32	3.0	0.0205
1D Celcon/Quartz	0.0060	3.32	6.5	0.0031

* Calculated from correlation data reported in Table 2; V = 4300 ft/sec; θ = 13.5 and 9 degrees for radome and antenna window materials, respectively.

4.0 POST-TEST EVALUATIONS

The actual test parameters are summarized in Table 4. It should be noted that the conditions for the IR domes were significantly different than for the radome and antenna window materials. Limited previous experience with MgF_2 domes indicated that the specified radome test conditions would be overly severe for this material in terms of both erosion resistance and thermal shock resistance. Therefore, the IR domes were tested in a separate run with the less severe environment listed in Table 4. The measured erosion rates (specimen midpoint recession rate and average mass loss rate) for the radome and antenna window materials are summarized in Table 5. The erosion performance of the radome and antenna window materials is discussed in Section 4.1, while the performance of the IR dome material is described in Section 4.2. Brief qualitative characterizations of the test environment and the model performance are presented in Sections 4.3 and 4.4, respectively.

Table 4. Test conditions.

	RADOMES AND ANTENNA WINDOWS	IR DOMES
Chamber Pressure, psi	938	996
Total Enthalpy (mass averaged), Btu/lbm	1648	505
Total Temperature, ^{o}R	5550	2618
Air Mach Number	8.4	9.4
Particle Type	Magnesium Oxide	Magnesium Oxide
Particle Diameter (nominal), microns	200	50
Particle Velocity, ft/sec	4400	3900
Particle Concentration, gm/m^3	2.5	0.6

4.1 RADOME AND ANTENNA WINDOW MATERIALS PERFORMANCE

4.1.1 Materials Ranking

The radome and antenna window materials each are ranked according to the measured specimen midpoint recession rate in Table 6. This midpoint recession rate was used instead of the mass loss rate to evaluate the erosion behavior of the materials because many of the materials eroded only at the specimen leading edge. This non-uniform erosion was caused by the different erosion behavior of the upstream silica phenolic holder material. Material densities are included in the rankings, since there is a strong correlation of erosion rate with material density.

Table 5. Summary of dust erosion test results.

Material	Specimen ID	Strut/ Position*	Wedge Angle (deg)	Pre-Heat Time θ_1 (sec)	Dust Time θ_2 (sec)	Pre-Test Thickness** t_1 (in)	Post-Test Thickness** t_2 (in)	Erosion $t_1 - t_2$ (in)	Pre-Test Mass M_1 (gm)	Post-Test Mass M_2 (gm)	Mass Loss $M_1 - M_2$ (gm)	Erosion Rate $(t_1 - t_2)/\theta_2$ (in/sec)	Mass Loss Rate $(M_1 - M_2)/\theta_2$ (gm/sec)	Remarks
Alumina	A3-5.0-3	1/1	13.5	25.3	5.05	0.170	0.170	0.0	13.0	12.9	0.1	0.0	0.020	Erosion at leading edge
Alumina	A3-5.0-4	1/2	13.5	25.3	5.05	0.170	0.170	0.0	13.0	12.9	0.1	0.0	0.020	Erosion at leading edge
Beryllia	A6-5.0-1	2/1	13.5	25.8	4.74	0.159	0.159	0.0	8.7	8.4	0.3	0.0	0.063	Erosion at leading edge
Beryllia	A6-5.0-3	2/2	13.5	25.8	4.74	0.170	0.169	0.001	9.2	9.0	0.2	0.0002	0.042	Erosion at leading edge
Pyroceram 9609	A1-5.0R-1 (E-15)	3/1	13.5	25.4	2.48	0.169	0.168	0.001	8.6	8.4	0.2	0.0004	0.081	Erosion at leading edge
Pyroceram 9609	A1-5.0R-2 (E-15)	3/2	13.5	25.4	2.48	0.170	0.169	0.001	8.7	8.4	0.3	0.0004	0.121	Erosion at leading edge
Pyroceram 9609	A1-5.0R-3 (E-16)	7B/1	9.0	25.2	1.35	0.169	0.169	0.0	8.6	8.5	0.1	0.0	0.074	Very slight erosion at leading edge
Rayceram Cordierite	A17-5.0-10	4/1	13.5	25.4	1.83	0.161	0.160	0.001	8.0	7.9	0.1	0.0005	0.055	Erosion at leading edge
Reaction Sintered Silicon Nitride	A42-5.0R-4	4/2	13.5	25.4	1.83	0.170	0.143	0.027	7.8	6.5	1.3	0.014	0.710	Uniform erosion
Slip Cast Fused Silica (Corning)	A36-5.0R-1	5/1	13.5	25.2	1.52	0.170	0.152	0.018	6.6	5.8	0.8	0.012	0.526	Uniform erosion
Slip Cast Fused Silica (Martin Marietta)	A73-5.0R-4	5/2	13.5	25.2	1.52	0.169	0.140	0.029	6.5	5.2	1.3	0.019	0.855	Uniform erosion
Ethyl Silicate/ 3D Quartz	A4-5.0R-7	6A/1	9.0	25.5	1.96	0.169	0.130	0.039	5.9	4.0	1.9	0.020	0.969	Erosion slightly higher forward
Ethyl Silicate/ 3D Quartz	A4-5.0R-8	6A/2	9.0	25.5	1.96	0.168	0.120	0.048	5.6	3.7	1.9	0.024	0.969	Erosion slightly higher forward
Isotropic Pyrolytic Boron Nitride	A6-4.0R-6	6B/1	9.0	25.5	1.96	0.167	0.114	0.053	4.4	3.0	1.4	0.027	0.714	Erosion slightly higher at midpoint
Isotropic Pyrolytic Boron Nitride	A6-4.0R-7	6B/2	9.0	25.5	1.96	0.170	0.114	0.056	4.6	3.2	1.4	0.029	0.714	Erosion slightly higher at midpoint
Jelly Roll Quartz/ Colloidal Silica	A41-5.0R-2	7A/1	9.0	25.2	1.35	0.169	0.150	0.019	5.6	4.2	1.4	0.014	1.037	Uniform erosion; corners chipped during post-test disassembly
Jelly Roll Quartz/ Colloidal Silica	A41-5.0R-3	7A/2	9.0	25.2	1.35	0.170	0.145	0.025	5.6	4.1	1.4	0.019	1.037	Uniform erosion; corners chipped during post-test disassembly
1-D Celcon/Quartz	A5-4.0R-8	7B/2	9.0	25.2	1.35	0.170	0.169	0.001	6.1	6.0	0.1	0.0007	0.074	Uniform erosion; very fine, filament roughness normal to surface

Notes:

* Specimen position identified in figure.

** Measurement made at specimen midpoint (X = 0.615) along centerline.

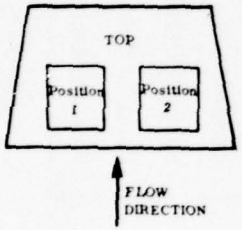

Table 6. Materials ranking.

RADOME MATERIALS

MATERIAL	DENSITY (GM/CC)	EROSION RATE (IN/SEC)
Alumina (Alsimag 753)	3.850	0.0000
Beryllia (Alsimag 754)	2.880	0.0001
Pyroceram 9606	2.599	0.0004
Rayceram Cordierite	2.510	0.0005
Slip Cast Fused Silica (Corning)	1.950	0.0120
Reaction Sintered Silicon Nitride	2.550	0.0140
Slip Cast Fused Silica (Martin Marietta)	1.918	0.0190

ANTENNA WINDOW MATERIALS

MATERIAL	DENSITY (GM/CC)	EROSION RATE (IN/SEC)
1D Celcon/Quartz	1.803	0.0007
Jelly Roll Quartz Colloidal Silica	1.650	0.0170
Ethyl Silicate/3D Quartz	1.748	0.0220
Isotropic Pyrolytic Boron Nitride	1.320	0.0280

The results in Tables 5 and 6 indicate that, for the present test conditions, alumina and beryllia are the most erosion-resistant materials tested. The performances of Pyroceram and Rayceram Cordierite also were very good. These four materials were substantially better than the other three candidate radome materials (the measured recession rate of the next best radome material was a factor of nearly 25 greater than the recession rate of Rayceram Cordierite) and should be included in any future evaluation and/or characterization programs.

Of the candidate antenna window materials, 1D Celcon/quartz clearly was the most erosion-resistant in the conditions tested (a factor of almost 25 lower recession rate than the next best material). Future evaluations of this material also should consider the compatibility of ablation performance and erosion resistance with representative heatshield materials in order to prevent the development of surface protuberances during flight.

4.1.2 Comparison of Dust Erosion With Equivalent Rain Erosion

In Section 3.3, dust erosion rates were predicted from the rain erosion data correlations. Because the actual test conditions (Table 4) were somewhat different from the specified conditions (Section 3.2), the measured dust erosion rates cannot be compared directly with the pre-test predicted erosion rates. The assumption was made that rain and dust erosion rates were the same in equivalent environments (V, ω, θ), and this assumption allowed pre-test dust erosion predictions to be made from rain data. This assumption can be checked by computing the erosion rates that the MDPR correlations would have predicted for the actual test conditions and comparing the results with the measured erosion rates. This was performed for the actual test parameters; i.e., V = 4400 ft/sec, $\omega = 2.51$ gm/m^3, and $\theta = 13.5$ degrees or 9 degrees. Again, the assumption was made that erosion rate varied linearly with the particle concentration, ω. The results are presented in Table 7.

In general, the results in Table 7 indicate that the relative erosion performance of the candidate materials is approximately the same in both rain and dust environments. That is, the materials that performed well in the rain environments also performed well in the dust erosion tests. However, the absolute magnitudes of the measured and predicted erosion rates are in generally poor agreement. The recession rate predictions based on the correlation expressions from the rain tests were found to underpredict the measured recession rates for some materials and to overpredict the recession rates for other materials. The discrepancies range from -100 percent to +710 percent. This lack of agreement strongly suggests that the existing correlation expressions are not suitable for performing flight response predictions of radome and antenna window materials in nuclear dust environments.

There are several possible reasons for the observed differences in the predicted and measured recession rates, and the very limited dust erosion data base precludes selection of the specific reason(s) at this time. Some portion of the difference certainly must be attributed to the differences in the types of particles. For example, water drops are affected more by the shock layer than are dust particles. The droplets tend to break up and/or vaporize in the shock layer, causing a reduction of the incident mass flux as well as more deceleration and deflection of the particles prior to surface impact. There also may be significant differences in details of the cratering phenomena produced by the different particle materials.

Other differences in the observed material responses in the rain and dust environments may be related to uncertainties in definition of the test environments. It was not possible in the

Table 7. Comparison of measured dust erosion and predicted equivalent rain erosion recession rates.

MATERIAL	MEASURED DUST EROSION (1)		PREDICTED EQUIVALENT RAIN EROSION (2)				PERCENT DIFFERENCE
	NUMBER OF TESTS	$\dot{S}_{DUST}$ (3) (IN/SEC)	VELOCITY (FT/SEC)	ANGLE (DEG)	CONCENTRATION RATIO, ω_p/ω (4)	$\dot{S}_{RAIN}$ (IN/SEC)	$100 \times \frac{\dot{S}_{DUST} - \dot{S}_{RAIN}}{\dot{S}_{RAIN}}$
Alumina (Alsimag 753)*	2	0.0000	4400.0	13.5	0.896	3.25×10^{-6}	-100
Beryllia (Alsimag 754)*	2	0.0001	4400.0	13.5	0.896	0.0003	-67
Ethyl Silicate/3D Quartz**	2	0.0220	4400.0	9.0	0.386	0.0166	33
Isotropic Pyrolytic Boron Nitride**	2	0.0280	4400.0	9.0	0.322	0.0155	81
Jelly Roll Quartz/Colloidal Silica**	2	0.0170	4400.0	9.0	0.386	0.0021	710
Pyroceram 9606*	2	0.0004	4400.0	13.5	0.837	0.0021	-81
Rayceram Cordierite*	1	0.0005	4400.0	13.5	0.896	0.0002	150
Reaction Sintered Silicon Nitride*	1	0.0140	4400.0	13.5	0.836	0.0063	122
Slip Cast Fused Silica* (Corning)	1	0.0120	4400.0	13.5	0.386	0.0067	79
Slip Cast Fused Silica* (Martin Marietta)	1	0.0190	4400.0	13.5	0.837	0.0166	145
1D Celcon/Quartz**	1	0.0007	4400.0	9.0	0.386	0.0027	-74

(1) DET test data
(2) Holloman track rain data
(3) $\dot{S}_{Dust}$ is the average for all of the tests
(4) Concentration ratio, ω_p/ω, is the ratio of the dust concentration to the rain concentration.
(5) $\dot{S}_{Rain}$ is based on Table 2 rain correlation data, tabulated velocity and angle, and concentration ratio. The assumption is made that erosion rate varies linearly with particle concentration.
(6) Material Code: * = Radome material
** = Antenna window material

present limited study to assess the precision with which the various flowfield and erosion parameters were measured at the Holloman sled facility. However, certain critical test parameters in the DET facility were subject to errors of unknown magnitude. (Some of these possible error sources are discussed briefly in the following section.) Thus, the material response predictions can be in error because of errors in the defined environment. For materials with very small recession rates, small errors in the absolute magnitude of the recession rate can produce relatively large discrepancies between the measured and predicted erosion performance.

In any event, it must be concluded at this time that the dust erosion response of radome and antenna window materials cannot be predicted with confidence by expressions based on tests performed in rain environments. Additional tests are therefore required to: 1) define the source(s) of the discrepancies more accurately, 2) expand the data base to obtain an estimate of the normal scatter in the measured erosion response, and 3) measure the erosion response as a function of changes in several key parameters (e.g., particle size, impact velocity, impact angle, and material temperature) in order to define more comprehensive erosion mass loss models for the materials of most interest.

4.2 IR DOME PERFORMANCE

The erosion performance of the magnesium fluoride (MgF_2) IR dome material was unsatisfactory in the present test environment (Table 4). Model SD-3, which had an initial thickness of 0.109 inch, fractured immediately following initiation of the particle flow. No portion of this model was available for post-test examination. The second model (SD-8), which had an initial thickness of 0.160 inch, survived the full duration test exposure of 10 seconds of clear air preheat and 2.75 seconds of particle flow. However, this model experienced complete burn-through in the stagnation region, as illustrated in Figure 5. (The time at which burn-through occurred is not known since motion picture coverage was not available for these two models.) A burn-through of this type in a flight environment would, of course, constitute a complete system failure since the internal components would be exposed to direct aerodynamic heating and particle impingement.

It also should be noted that, even if the particle flow had ended before burn-through occurred, the performance of the IR sensor probably would be degraded significantly as a result of the particle-induced surface roughness on the dome (Figure 5). To quantify this effect, the infrared transmission characteristics of the surface were measured before and after the test. It was found that the post-test transmittance in the wave length band of interest was less than one-third

of the pre-test value. Thus, traversal of a dust cloud equivalent to the DRT environment can have an adverse effect on system performance as well as compromising vehicle survivability.

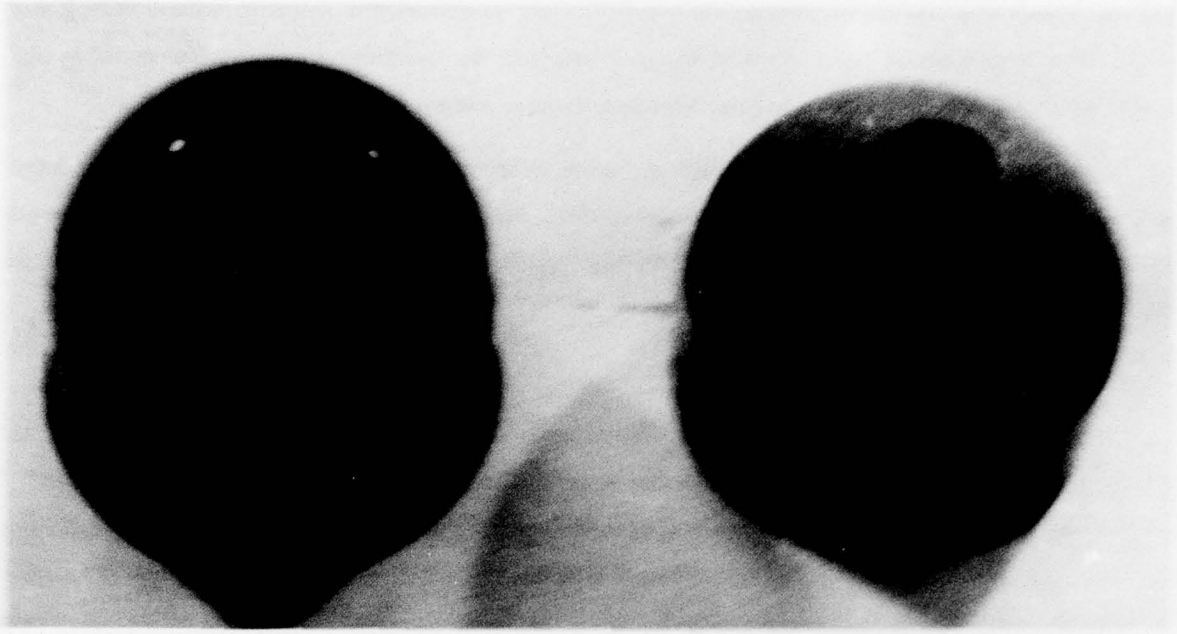

PRE-TEST POST-TEST

Freestream particle concentration is determined from the total mass of particles injected and the total time of particle injection. Such an average does not account for particle flow transients which are caused by turning the particle flow on and off for short durations throughout the run. For a very short burst of particles (~1 second), the particle concentration could be significantly different than the average concentration for the entire run.

Although not used in this program, laser holograms of the particle environment have been used at AEDC to evaluate particle size, velocity, and concentration. Such a method of evaluation should be employed in any future tests of this type to obtain a more accurate characterization of the erosion environment.

4.4 TEST MODEL DESIGN ASSESSMENT

The overall performance of the wedge model design was satisfactory. The wedge surface assembly can be modified slightly to improve the ablation uniformity of the test specimen. The silica phenolic retainer plate upstream of many specimens eroded at a different rate from the specimen. This resulted in non-uniform erosion at the sample leading edge. Replacing the silica phenolic just upstream of the test sample with a small, separate piece of sample material will greatly reduce non-uniform erosion at the leading edge.

5.0 CONCLUSIONS

A limited ground test program was conducted to obtain a preliminary assessment of the performance of several candidate radome and antenna window materials in a simulated nuclear dust environment. An alternate objective of the program was to compare the dust erosion performance of the materials to the more extensive results for the same materials in rain erosion tests. The tests were performed in the Dust Erosion Tunnel at AEDC at conditions similar to those used in the rain erosion tests. Comparisons with the measured results were made with erosion expressions derived from the rain data.

The results of the tests indicated substantial differences in performance among the candidate materials. Alumina and beryllia were the most erosion-resistant radome materials in the DET test environment, although Pyroceram and Rayceram Cordierite also performed very well. The erosion performance of the other three candidate radome materials was significantly worse than the performance of these four materials. Similarly, 1D Celcon/quartz exhibited much greater erosion resistance in these test conditions than the other three candidate antenna window materials.

This relative performance of the materials is in general agreement with the qualitative performance rankings predicted by the rain erosion test results. However, the magnitudes of the measured recession rates are substantially different than the rates that were predicted with correlation equations based on rain test data. Thus, the rain-based expressions cannot be used to design radomes and antenna window materials for survival in nuclear dust environments. Although there are several possible explanations for this discrepancy, the present data base is too limited to permit accurate definition of the different response mechanisms in the two types of erosive environments.

Two samples of one infrared (IR) dome material of current interest (magnesium fluoride) also were tested in an erosive environment of less severity than was used for the preceding materials. The erosion performance of this IR dome material was found to be unsatisfactory in the test environment. One model fractured upon initial exposure to the particle flow and was completely destroyed. The second model experienced complete burn-through in the stagnation region after a 2.75-second exposure to the particle flow. In addition, the dome surface was severely roughened by the particle impacts and the resultant infrared transmittance of the material was less than one-third the transmittance of the virgin material. Additional tests are required to define the erosion response and transmittance characteristics of the magnesium fluoride dome material as a function of the severity of the erosive environment. The vulnerability of these window materials

probably lies in the transmittance losses associated with low density dust encounters, more typical of a dusty battlefield than the DET environment.

REFERENCES

1. Lewis, H. F., Patton, J. B., Horn, D. C., et al., "Description of the AEDC Erosion Tunnel," AEDC-TR-73-74, May 1973.

2. Schmitt, G. F., Jr., and Krabill, A. H., "Velocity-Erosion Rate Relationships of Materials in Rain at Supersonic Speeds," AFML-TR-70-44, October 1970.

3. Schmitt, G. F., Jr., "*Multiple Impingement* Rain Erosion Behavior of Reentry Vehicle Carbon-Carbon and Quartz/Silica Composite Materials and Monolithic Ceramic Radome Materials," AFML-TR-75-74, October 1975.

4. Schmitt, G. F., Jr., Reinecke, W. G., and Waldman, G. D., "Influence of Velocity, Impingement Angle, Heating, and Aerodynamic Shock Layers on Erosion of Materials at Velocities of 5500 ft/s (1700 m/s)," American Society for Testing and Materials Special Technical Publication 567, 1975.

5. Schmitt, G. F., Jr., "Influence of Materials Construction Variables on the Rain Erosion *Performance of Carbon-Carbon Composites, Heat Shields and Radome* Materials," AFML-TR-76-203, February 1977.

APPENDIX A

MODEL PHOTOGRAPHS

Pre-test and post-test photographs of the model erosion surfaces are presented to allow qualitative comparisons to be made between materials. The pre-test photographs include the specimen identifications. The pre-test specimen positions are preserved in the post-test photographs. Non-uniform erosion can be seen best from the post-test photographs which show perspective views of the erosion surfaces.

Photographs are presented in Figures A1 through A9. Material and strut/position identifications are included in the figure titles.

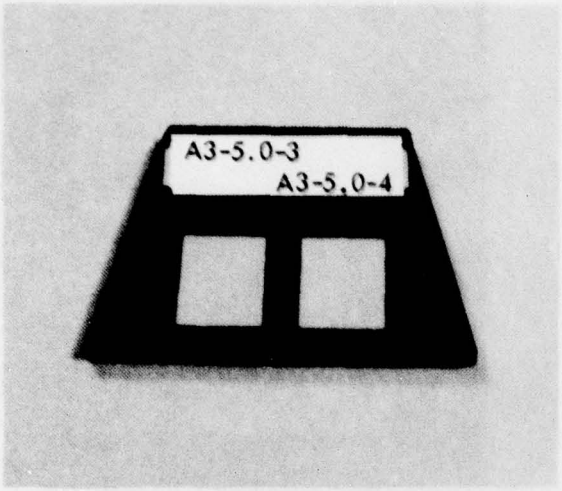

PRE-TEST

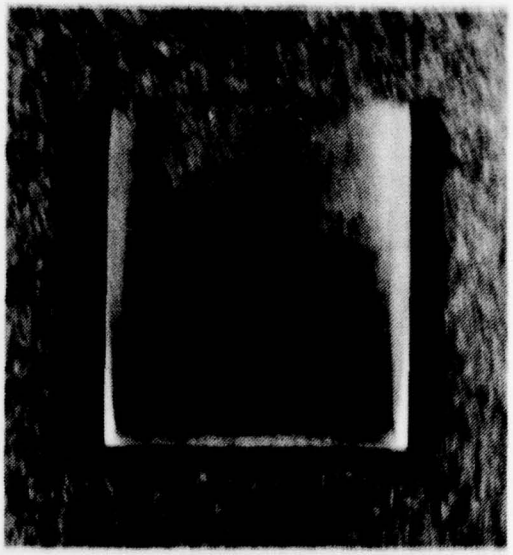

POST-TEST
ALUMINA
POSITION 1

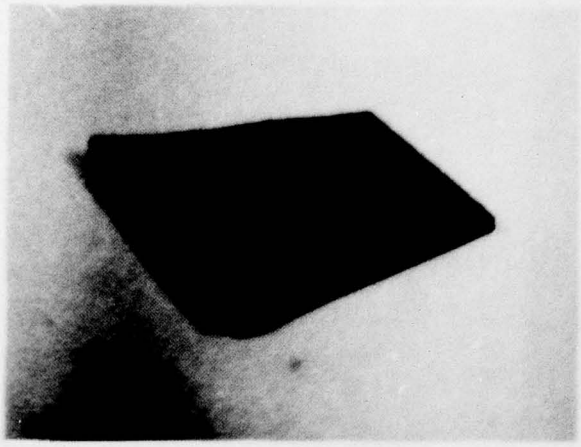

POST-TEST

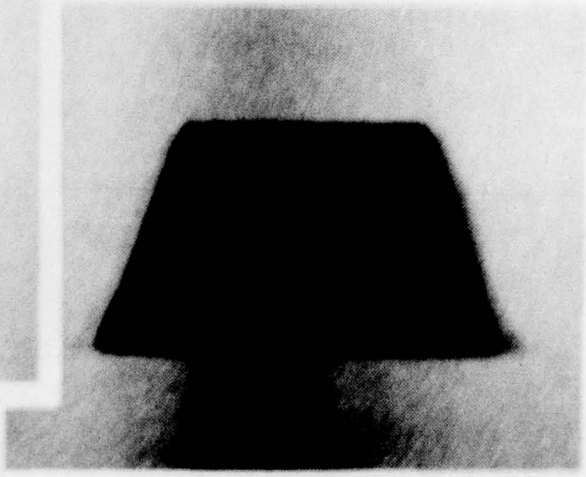

Figure A1. Pre- and post-test photographs of Alumina (Strut 1, Positions 1 and 2).

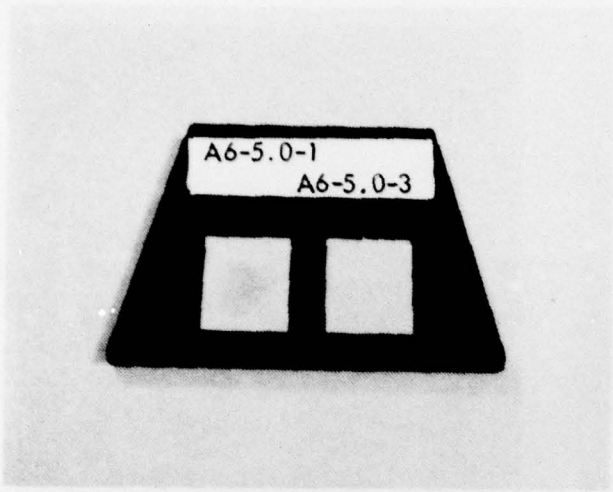

PRE-TEST

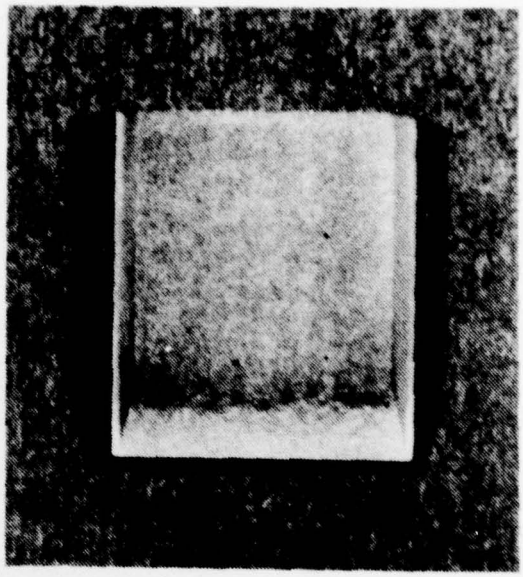

POST-TEST
BERYLLIA POSITION 1

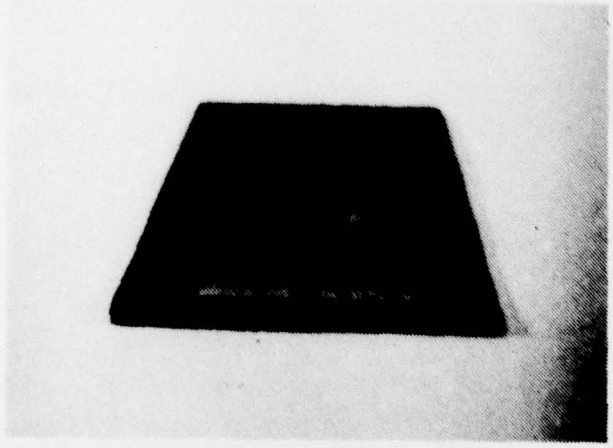

POST-TEST

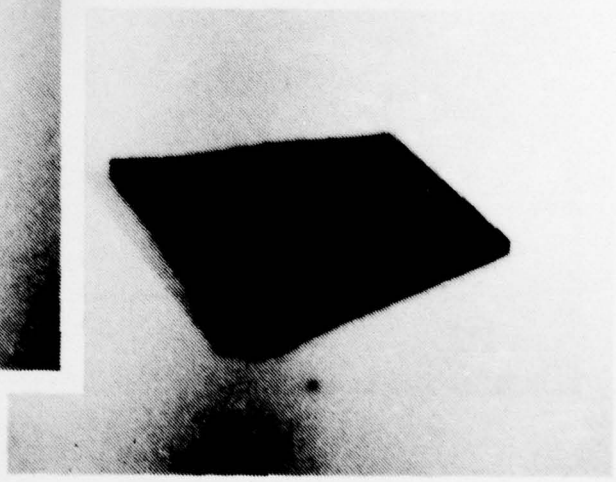

T800123

Figure A2. Pre- and post-test photographs of Beryllia (Strut 2, Positions 1 and 2).

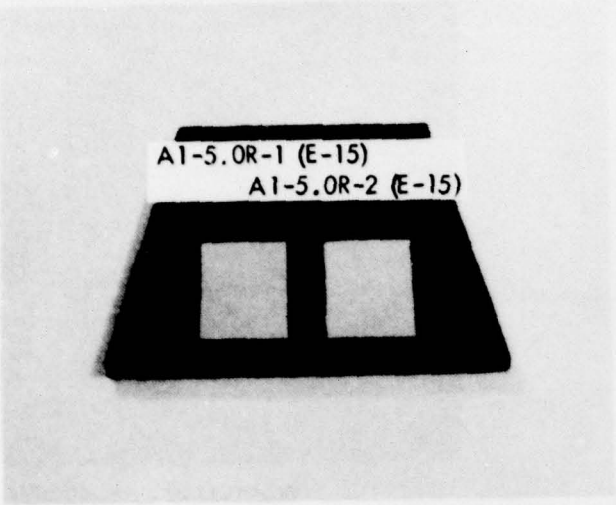

PRE-TEST

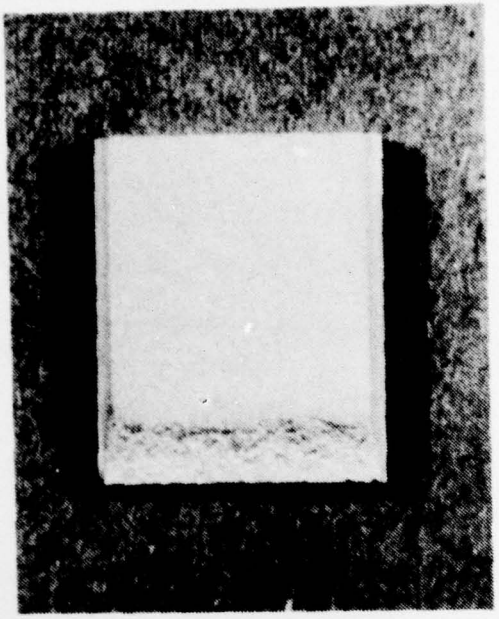

POST-TEST
PYROCERAM POSITION 1

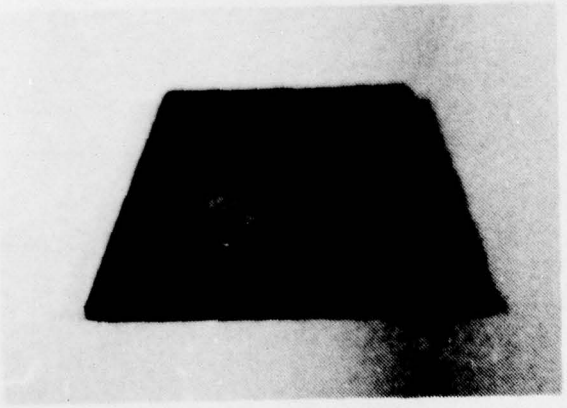

POST-TEST

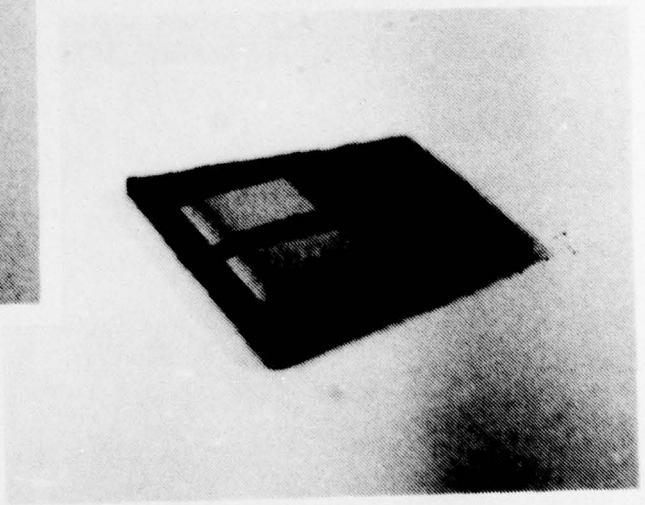

7800123

Figure A3. Pre- and post-test photographs of Pyroceram 9606 (Strut 3, Positions 1 and 2).

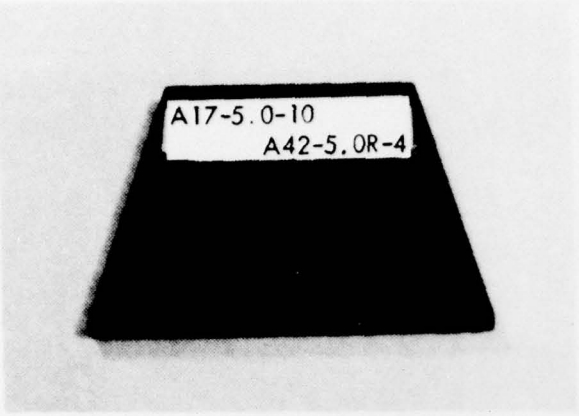

PRE-TEST

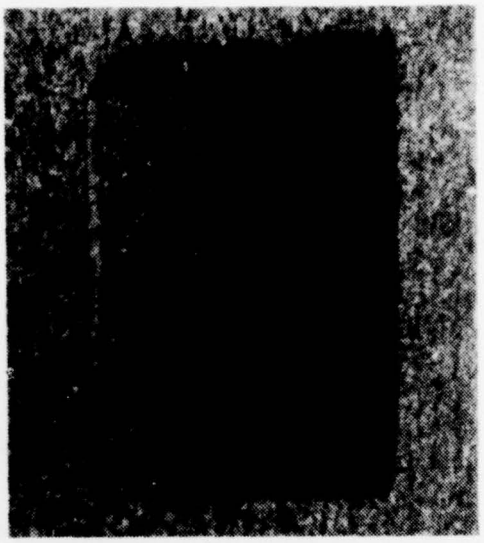

POST-TEST
REACTION SINTERED
SILICON NITRIDE
POSITION 2

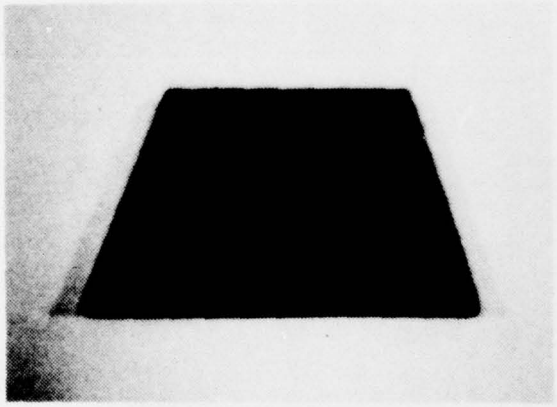

POST-
TEST

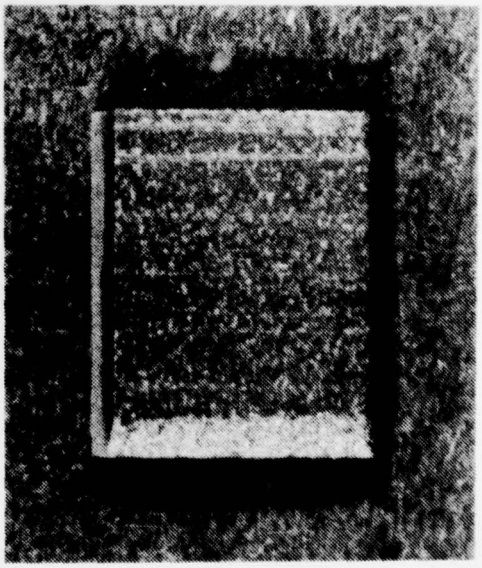

POST-TEST
RAYCERAM
CORDIERITE
POSITION 1

7800117

Figure A4. Pre- and post-test photographs of Rayceram Cordierite (Strut 4, Position 1) and Reaction Sintered Silicon Nitride (Strut 4, Position 2).

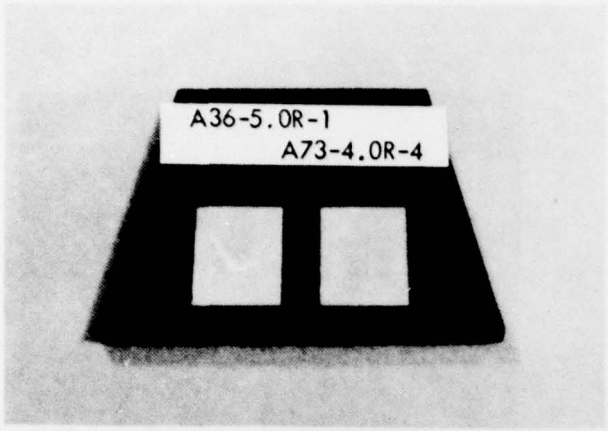

PRE-TEST

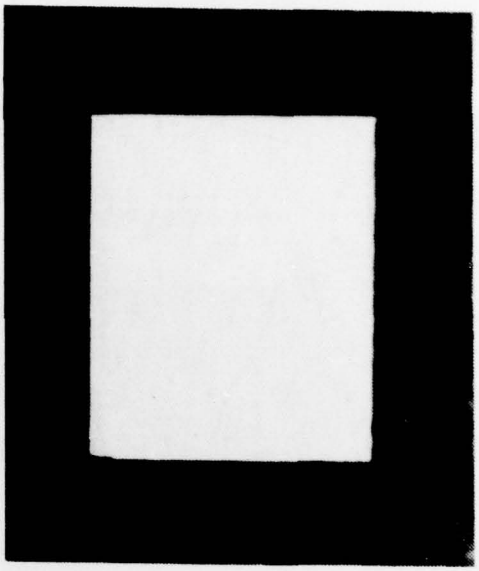

POST-TEST
SLIP CAST
FUSED SILICA
(MARTIN MARIETTA)
POSITION 2

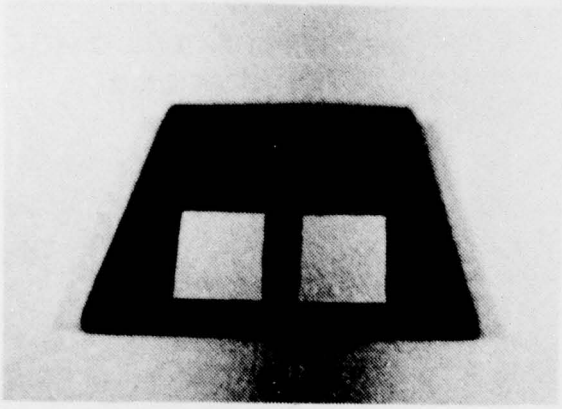

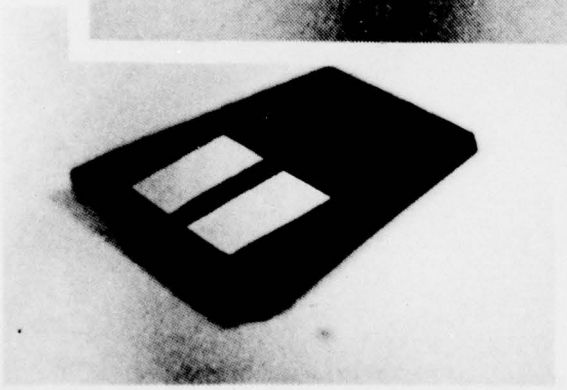

POST-
TEST

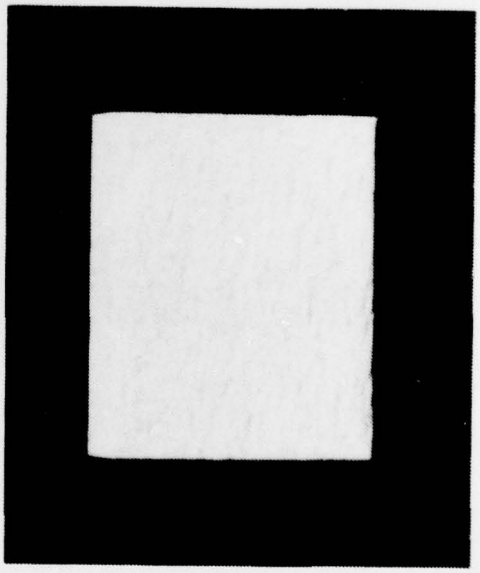

POST-TEST
SLIP CAST
FUSED SILICA
(CORNING)
POSITION 1

7800123

Figure A5. Pre- and post-test photographs of Slip Cast Fused Silica: Corning (Strut 5, Position 1) and Martin Marietta (Strut 5, Position 2).

PRE-TEST

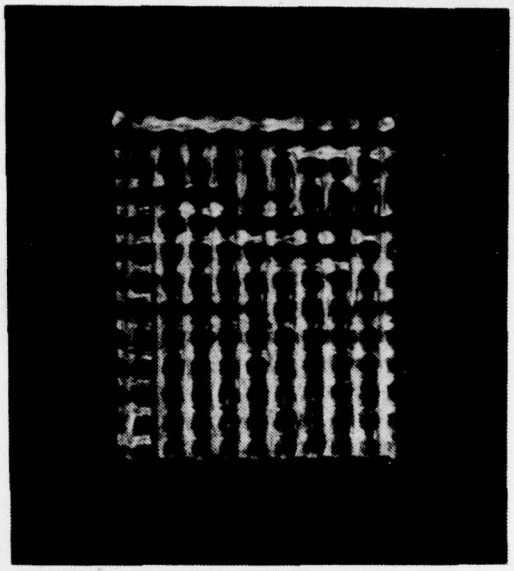

POST-TEST
ETHYL SILICATE/3D QUARTZ
POSITION 2

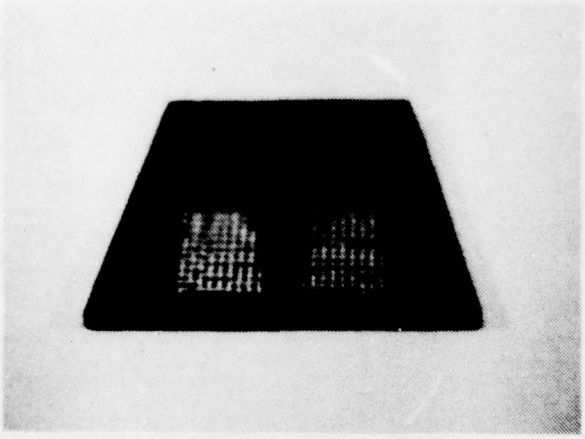

POST-TEST

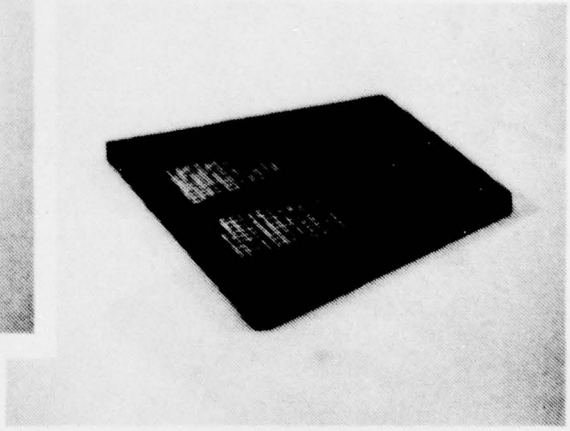

7800120

Figure A6. Pre- and post-test photographs of Ethyl Silicate/3D Quartz (Strut 6A, Positions 1 and 2).

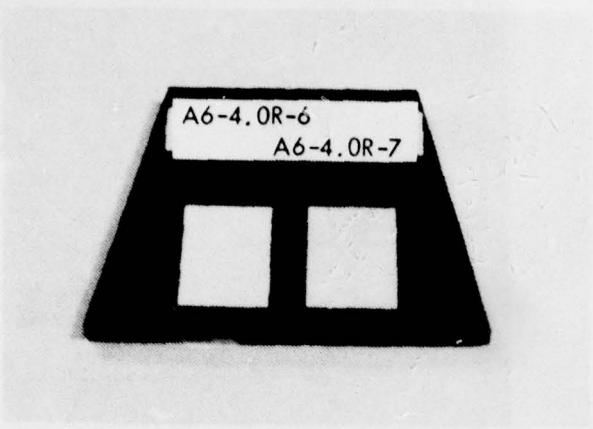

PRE-TEST

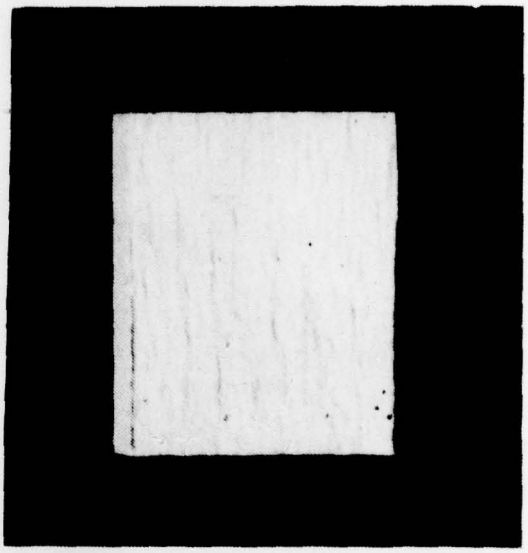

POST-TEST
ISOTROPIC PYROLYTIC
BORON NITRIDE
POSITION 2

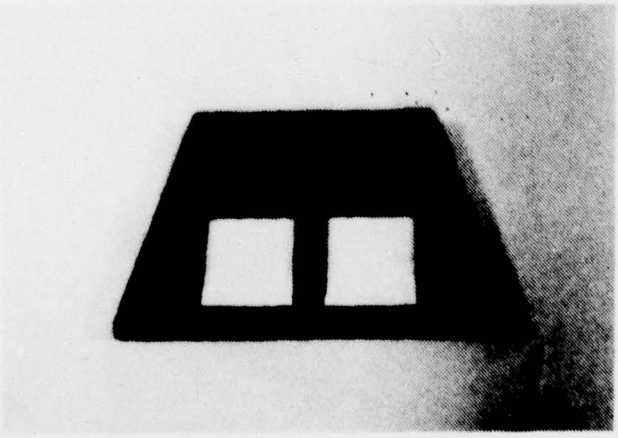

POST-TEST

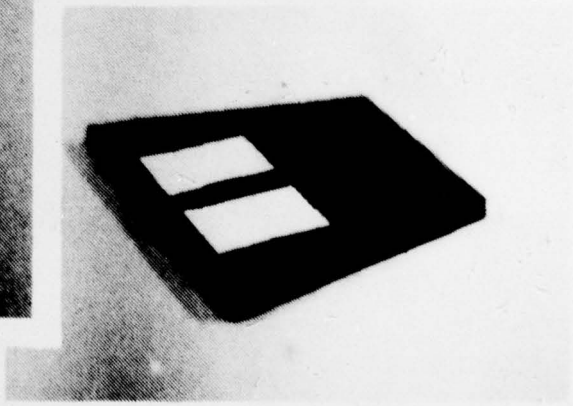

Figure A7. Pre- and post-test photographs of Isotropic Pyrolytic Boron Nitride (Strut 6B, Positions 1 and 2).

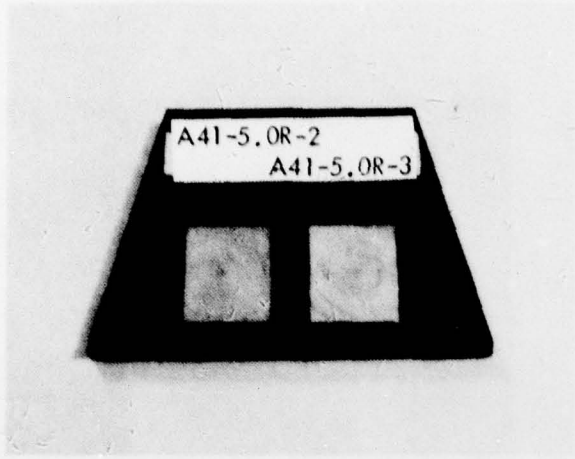

PRE-TEST

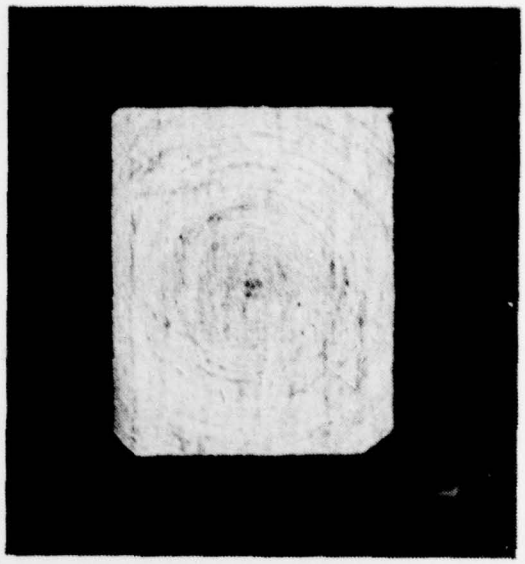

POST-TEST
JELLY ROLL QUARTZ/
COLLOIDAL SILICA
POSITION 2

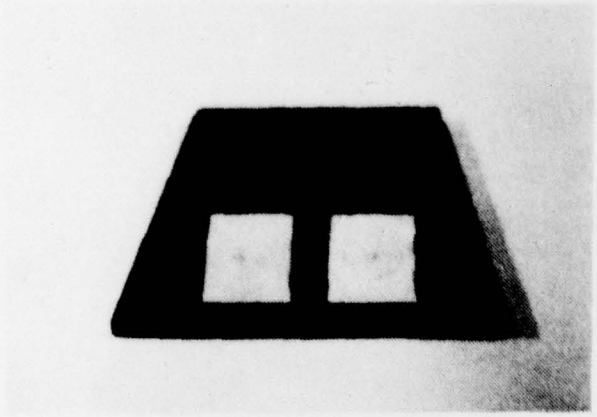

POST-TEST

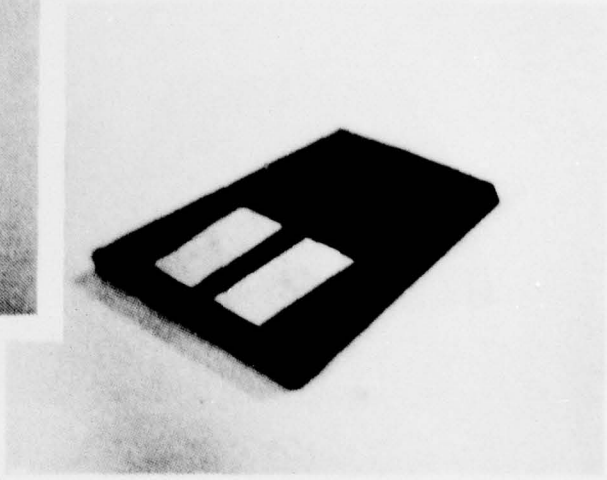

Figure A8. Pre- and post-test photographs of Jelly Roll Quartz/ Colloidal Silica (Strut 7A, Positions 1 and 2).

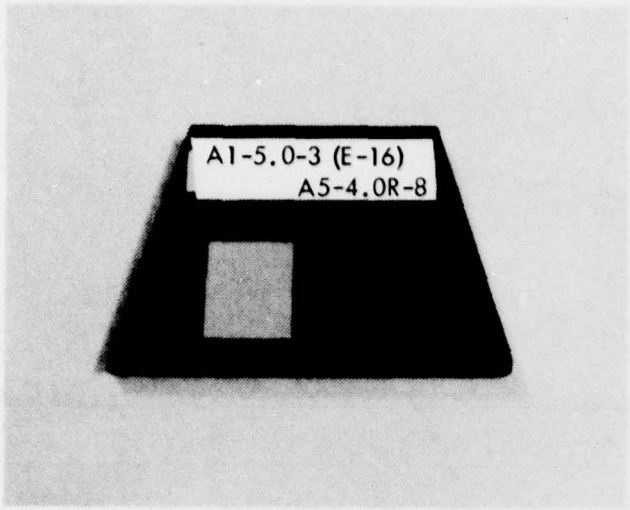

PRE-TEST

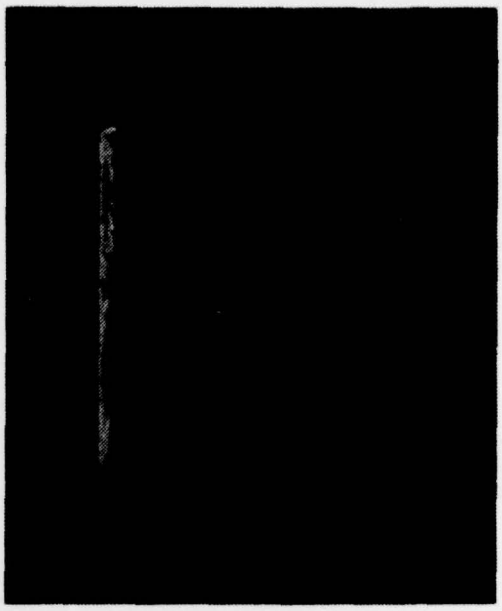

POST-TEST
1D CELCON/QUARTZ
POSITION 2

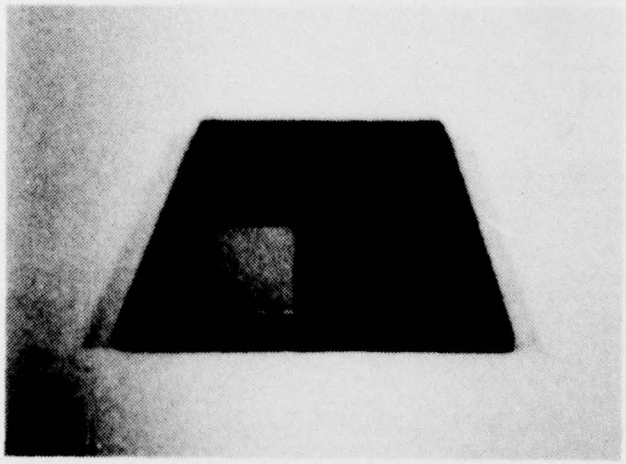

POST-TEST

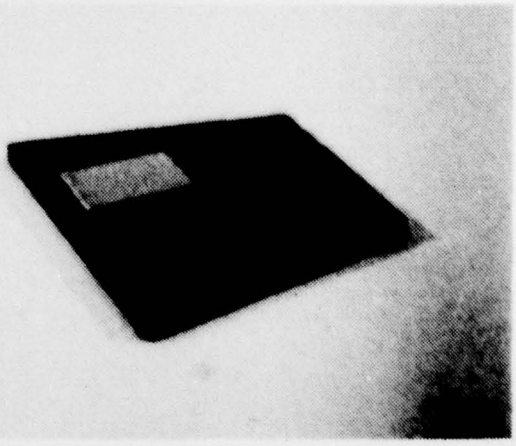

7800122

Figure A9. Pre- and post-test photographs of Pyroceram 9606 (Strut 7B, Position 1) and 1D Celcon/quartz (Strut 7B, Position 2).

DISTRIBUTION LIST

DEPARTMENT OF DEFENSE

Assistant to the Secretary of Defense
Atomic Energy
ATTN: Executive Assistant

Defense Documentation Center
12 cy ATTN: DD

Defense Intelligence Agency
ATTN: DT-1C
ATTN: DB-4D
ATTN: DT-2
ATTN: DT-2, T. Dorr

Defense Nuclear Agency
2 cy ATTN: SPAS
4 cy ATTN: TITL
ATTN: DDST
ATTN: RATN
ATTN: STVL

Field Command
Defense Nuclear Agency
ATTN: FCTMOF
ATTN: FCPR

Field Command
Defense Nuclear Agency
Livermore Division
ATTN: FCPRL

Joint Chiefs of Staff
ATTN: J-5, Nuclear Division
ATTN: SAGA/SFD
ATTN: SAGA/SSD

Joint Strat. Tgt. Planning Staff
ATTN: JPST, G. Burton
ATTN: JPST
ATTN: JLTW-2
ATTN: JPTM

NATO School (SHAPE)
ATTN: U.S. Documents Officer

Undersecretary of Defense for Rsch. & Engrg.
ATTN: Strategic & Space Systems (OS)

DEPARTMENT OF THE ARMY

BMD Advanced Technology Center
Department of the Army
ATTN: ATC-T, M. Capps

BMD Systems Command
Department of the Army
ATTN: BMDSC-H, N. Hurst

Deputy Chief of Staff for Rsch. Dev. & Acq.
Department of the Army
ATTN: DAMA-CSS-N

Harry Diamond Laboratories
Department of the Army
ATTN: DELHD-N-P

DEPARTMENT OF THE ARMY (Continued)

U.S. Army Ballistic Research Labs
ATTN: DRDAR-BLT, R. Vitali
ATTN: DRDAR-BL, R. Eichelberger

U.S. Army Material & Mechanics Rsch. Ctr.
ATTN: DRXMR-HH, J. Dignam

U.S. Army Missile R & D Command
ATTN: DRDMI-TRR, B. Gibson

U.S. Army Nuclear & Chemical Agency
ATTN: Library

U.S. Army Research Office
ATTN: P. Radowski, Consultant

U.S. Army TRADOC Systems Analysis Activity
ATTN: ATAA-TDC, R. Benson

DEPARTMENT OF THE NAVY

Naval Research Laboratory
ATTN: Code 7908, A. Williams

Naval Surface Weapons Center
ATTN: Code K06, C. Lyons
ATTN: Code F31

Office of the Chief of Naval Operations
ATTN: OP 604E14, R. Blaise

Strategic Systems Project Office
Department of the Navy
ATTN: NSP-273
ATTN: NSP-272

DEPARTMENT OF THE AIR FORCE

Air Force Materials Laboratory
ATTN: MBC, D. Schmidt
ATTN: MBE, G. Schmitt

Air Force Systems Command
ATTN: SOSS
ATTN: XRTO

Air Force Technical Applications Center
ATTN: TF

Air Force Weapons Laboratory, AFSC
ATTN: SUL
ATTN: ALO, L. James
ATTN: DES, G. Ganong

Deputy Chief of Staff
Operations Plans and Readiness
Department of the Air Force
ATTN: AFXOOSS

Deputy Chief of Staff
Research, Development, & Acq.
Department of the Air Force
ATTN: AFRDQSM

DEPARTMENT OF THE AIR FORCE (Continued)

Foreign Technology Division, AFSC
Department of the Air Force
ATTN: SDBS, J. Pumphrey

Space & Missile Systems Organization
Air Force Systems Command
ATTN: MNN

Space & Missile Systems Organization
Air Force Systems Command
ATTN: RSSE

Strategic Air Command
Department of the Air Force
ATTN: XPFS
ATTN: XPQM
ATTN: XOBM

DEPARTMENT OF ENERGY CONTRACTOR

Sandia Laboratories
Livermore Laboratory
ATTN: Doc. Con. for T. Cook

DEPARTMENT OF DEFENSE CONTRACTORS

Acurex Corporation
ATTN: R. Kendall
ATTN: C. Nardo

Aeronautical Rsch. Assoc. of Princeton, Inc.
ATTN: C. Donaldson

Aerospace Corporation
ATTN: R. Mortensen
ATTN: D. Glenn

AVCO Research & Systems Group
ATTN: W. Reinecke

California Research & Technology, Inc.
ATTN: K. Kreyenhagen
ATTN: M. Rosenblatt

Effects Technology, Inc.
ATTN: J. Carlyle
ATTN: F. Bick

DEPARTMENT OF DEFENSE CONTRACTORS (Continued)

General Electric Company
Re-Entry & Environmental Systems Division
ATTN: P. Cline
ATTN: B. Maguire

General Electric Company-TEMPO
ATTN: DASIAC
ATTN: B. Gambill

Harold Rosenbaum Associates, Inc.
ATTN: G. Weber

Kaman Sciences Corporation
ATTN: J. Harper

Lockheed Missiles & Space Company, Inc.
ATTN: A. Collins

Prototype Development Associates, Inc.
ATTN: J. McDonald
5 cy ATTN: E. Alexander
5 cy ATTN: M. Sherman

R & D Associates
ATTN: C. MacDonald
ATTN: F. Field

Rand Corporation
ATTN: R. Rapp

Science Applications, Inc.
ATTN: J. Stoddard

Science Applications, Inc.
ATTN: W. Seebaugh
ATTN: J. Cockayne

TRW Defense & Space Systems Group
ATTN: A. Zimmerman

TRW Defense & Space Systems Group
ATTN: W. Polich